npj | regenerative medicine

Article

Published in partnership with the Australian Regenerative Medicine Institute

https://doi.org/10.1038/s41536-025-00447-6

Long-term evaluation of human iPSC-derived cartilage for repairing chondral defects

Yangfan Lu[1,2], Elizabeth R. Kats[1,3], Sophie E. Hines[1,3], Jiangyinzi Shang[1], Shotaro Kamijo[1,4], Jia-Jun Liu[5,6], Silvia Liu[5,6], MaCalus V. Hogan[1,3,7] ✉ & Hang Lin[1,3,7] ✉

Induced pluripotent stem cells (iPSCs) have demonstrated superior capacity to regenerate hyaline cartilage compared to mesenchymal stromal cells (MSCs). However, most previous animal studies have only conducted short-term assessments. We performed a long-term (8 weeks) in vitro chondrogenesis of human iPSC-derived multipotent progenitor cells (iMPCs) and human MSCs. The expression levels of hypertrophy-related genes were significantly lower in the iMPC group compared to the MSC group, such as collagen type X being 5-fold lower on day 56. In the animal study, implants from the iMPC group maintained more matrix than the MSC group at both short and long-term time points (12 and 48 weeks). Importantly, at 48 weeks, the native cartilage surrounding the defect areas in some rats from the MSC group showed severe degradation, which was not observed in the iMPC group. In conclusion, iMPCs represent a safe and effective cell source for long-term hyaline cartilage repair.

Due to the avascular nature and limited self-healing capacity of hyaline cartilage, large cartilage defects require chondrocyte implantation or osteochondral transplantation to aid the repair process. Autologous chondrocyte implantation (ACI) is the most commonly used cell-based therapy in clinical settings. This approach involves the isolation, expansion, and reimplantation of autologous chondrocytes. However, ACI has limitations, including low availability of donor tissue, donor site morbidity, and the loss of chondrocyte phenotype during in vitro expansion. Consequently, researchers have explored other cell types for cartilage regeneration, such as stem cells and nasal chondrocytes[1]. Specifically, mesenchymal stem cells (MSCs) from various sources have demonstrated the ability to differentiate into chondrocyte-like cells[2]. However, this process often led to hypertrophic conversion, which resulted in tissue fibrosis, ossification, and apoptosis of the differentiated cells[3]. In contrast, hypertrophic conversion is not observed in native, healthy articular cartilage and chondrocytes.

Recently, induced pluripotent stem cells (iPSCs) have emerged as a potential alternative cell source for generating articular cartilage, with their potential being tested in both preclinical models and human studies[4]. It is important to note that there are various methods for creating chondrocytes from iPSCs, as summarized in a recent review[5], but a standardized and recognized approach has not yet been established. Additionally, while primary MSCs can form cartilage tissues when stimulated by transforming growth factor-β (TGFβ), iPSC-derived multipotent cells typically require stimulation from bone morphogenetic proteins (BMPs), either during the early differentiation of iPSCs to iPSC-derived multipotent progenitor cells (iMPCs) or embryoid bodies, or from iMPCs to chondrocytes[6,7]. For instance, in one of our recent studies, we discovered that a chondrogenic medium supplemented with TGFβ and bone morphogenetic protein 6 (BMP6) resulted in robust cartilage formation with minimal hypertrophy from iMPCs[8]. Additionally, the cartilage generated from iPSCs exhibited resistance to osteogenic transition when implanted subcutaneously, resulting in hyaline cartilage-like regeneration in osteochondral defects in rats.

Currently, both MSCs and iPSCs have been investigated for their potential in regenerating cartilage following acute chondral injury. However, the long-term viability of cartilage derived from MSCs or iPSCs, as well as its ability to maintain the hyaline phenotype over time, has not yet been fully explored. To the best of our knowledge, the longest assessed duration

[1]Department of Orthopaedic Surgery, University of Pittsburgh School of Medicine, Pittsburgh, PA, USA. [2]Xiangya Hospital, Central South University, Changsha, Hunan, China. [3]Department of Bioengineering, University of Pittsburgh Swanson School of Engineering, Pittsburgh, PA, USA. [4]Department of Pharmacology, Toxicology and Therapeutics, Division of Physiology, Showa Medical University School of Pharmacy, Tokyo, Japan. [5]Department of Pharmacology and Chemical Biology, University of Pittsburgh School of Medicine, Pittsburgh, PA, USA. [6]Organ Pathobiology and Therapeutics Institute, University of Pittsburgh School of Medicine, Pittsburgh, PA, USA. [7]Orland Bethel Family Musculoskeletal Research Center, University of Pittsburgh School of Medicine, Pittsburgh, PA, USA. ✉e-mail: hoganmv@upmc.edu; hal46@pitt.edu

has been limited to 6 months in mice[9] and 7 years in humans[10]. This is a critical issue, as patients receiving cell therapy expect the cartilage tissue to last for decades. The current study aimed to examine the efficacy and safety of iPSC-derived cartilage after implantation over an extended period, specifically 48 weeks in rats, which represents approximately 30-40% of their lifespan[11].

In this study, we first optimized the culture conditions and evaluated in vitro chondrogenesis at different time points, extending to 8 weeks. We then implanted these in vitro-generated cartilage tissues into osteochondral defects in rats. Histology and immunostaining techniques were employed to assess the phenotype of the regenerated tissues. Lastly, we examined the changes in the host cartilage to evaluate the effect of the implants. Our studies provide crucial information regarding the long-term efficacy and safety of both human MSCs and iPSC-derived cartilage, which is vital for informing future clinical applications.

Results

Cartilage generated by iPSCs displays lower hypertrophy levels than that from MSCs

Previously, we found that the combination of BMP4 + TGFβ3 displayed a comparable capacity as BMP6 + TGFβ3 to induce chondrogenesis of human multipotent cells from iPSCs (iMPCs)[8]. In that earlier study, the test was conducted over a 21-day culture period, and a longer culture time was not examined. Here, we first cultured human iMPCs in a chondrogenic medium containing either BMP4 + TGFβ3 or BMP6 + TGFβ3 for 56 days to compare the long-term efficacy of these two conditions in promoting cartilage formation. As shown in Supplementary Fig. 1, iMPCs were positive for CD73, CD90, and CD105, and negative for CD31, CD34 and CD45, which also were able to differentiated into chondrocytes, osteoblasts, and adipocytes. After 56 days of chondrogenesis, cartilage tissue derived from treatment with the combination of BMP4 + TGFβ3 displayed higher expression of collagen type II alpha 1 chain (*COL2A1)* and aggrecan (*ACAN*), as well as more deposition of Glycosaminoglycan (GAGs) (Supplementary Fig. 2). Therefore, all studies described below used the chondrogenic medium containing BMP4 and TGFβ3 to induce iMPC chondrogenesis.

We then monitored the longitudinal changes in iMPCs during the chondrogenic process for an extended period (up to 56 days, Fig. 1a), where MSCs were employed as a control. We first used qRT-PCR to measure the expression levels of genes associated with chondrogenesis and chondrocytic hypertrophy. For the MSC group, the expression levels of *COL2A1* and *ACAN* peaked at day 28 (Fig. 1b, c). For the iMPC group, the highest expression of these two genes was on day 56. Interestingly, levels of collagen type X alpha 1 chain (*COL10A1*) and osteocalcin (*BGLAP*) genes continued to elevate throughout the 56-day culture period in both MSC and iMPC cultures, although the expression levels were significantly higher in the MSC group (Fig. 1d, e, g). As a comparison, Runt-related transcription factor 2 (*RUNX2*) expression slightly increased over time, reaching the highest levels on day 28 for both groups; however, constructs from the iMPC group displayed lower expression levels than the MSC group in all tested time points (Fig. 1f). Results from western blot analyses confirmed that cartilage derived from iMPCs exhibited lower Runx2 levels than those from MSCs (Fig. 1h). It should be noted that MSCs rapidly produced high levels of SRY-Box transcription factor 9 (SOX9) and Runx2 proteins after 7 days of chondrogenic culture, while iMPCs displayed a delayed response to the treatment.

We then used histology and immunostaining to further examine the prosperities of MSC and iMPC-derived cartilage (Fig. 2). In general, the deposition of cartilage matrix, including glycosaminoglycans (GAGs) and Type II Collagen (COL2), increased with culture time. Importantly, cartilage created by iMPCs displayed minimal production of Type X Collagen (COL10), indicating a low hypertrophy phenotype. Under the chondrogenic culture conditions, we observed no bone formation in either group (Supplementary Fig. 3).

Cartilage generated by iPSCs displays lower apoptosis levels than that from MSCs

An important change related to chondrocytic hypertrophy is apoptosis[12]. We first used qRT-PCR to measure the expression levels of representative apoptosis genes (Fig. 3a–c). B-cell lymphoma 2 (*BCL2)* gene was significantly upregulated on day 21, reached its peak on day 28, and then decreased on day 56 in both cultures. However, its levels were lower in the iMPC group. Expression of caspase 3 (*CASP3*) and 8 (*CASP8*) increased on day 7 in the iMPC culture and remained stable throughout the culture. Western blot analysis further demonstrated that tissues in the MSC group exhibited higher BCL2 and caspase-3 levels than the iMPC group (Fig. 3f). Lastly, we used TUNEL staining to analyze the apoptosis levels. Cartilage tissues generated from MSCs on day 56 contained a large number of apoptotic cells (Fig. 3d, e). In contrast, very few iMPC-derived chondrocytes underwent apoptosis.

Taken together, after a long-term (56 days) in vitro chondrogenesis, MSC-derived cartilage displayed higher hypertrophy and apoptosis levels when compared to those from iMPC.

Cartilage generated by iPSCs generates fewer histocompatibility complex proteins and cytokines than that from MSCs

We used bulk RNA sequencing to further examine the difference in transcriptome between MSC and iMPC-derived cartilage after 56 days of chondrogenesis. The volcano plot showed that the global gene expression profiles of these two types of cartilage tissues were significantly different (Fig. 4a). Specifically, 787 genes were upregulated, and 772 genes were downregulated in chondrocytes derived from iMPCs compared to those from MSCs. Principal component analyses (PCA) placed MSC- and iMPC-derived chondrocytes in two distinct clusters, suggesting that they were genomically distinct (Fig. 4b).

Next, we performed functional annotation analyses of these differentially regulated genes to determine the enrichment of Gene Ontology (GO) terms and molecular pathways. The GO analyses demonstrated significant enrichment of several biological processes in MSC-derived chondrocytes, including major histocompatibility complex (MHC) proteins, collagen catabolic, cytokine production, and inflammatory (Fig. 4c). We also performed Kyoto Encyclopedia of Genes and Genomes (KEGG) pathway analysis, and results showed that cGMP-PKG, MAPK, Notch, PI3K-Akt, Ras, JAK-STAT, and Wnt pathways are the most different pathways between MSC and iMPC-derived chondrocytes (Fig. 4d).

Cartilage implants generated by iPSCs maintain a hyaline phenotype without negatively impacting native tissues

We next assessed the reparative capacity of MSC and iMPC-derived cartilage in vivo. Specifically, MSC or iMPC pellets were subjected to 56 days of chondrogenesis in vitro using the conditions described above and then implanted in osteochondral defects surgically created in the knees of adult rats. In this study, we used normal animals with intact immune functions to better simulate the situations in future clinical applications.

At the 12-week time point, macroscopic views of all samples are shown in Supplementary Fig. 4. In general, the iMPCs group exhibited better cartilage formation with less bloody tissue presence. In Fig. 5a, the samples that displayed the best and worst repair effects from both groups are shown. It is noticed that tissues within the defects from the iMPC group exhibited more deposition of Type II Collagen (COL2) and GAGs than the MSC group. In contrast, higher levels of Type I Collagen (COL1) and osteocalcin (OCN) were found in the MSC group, suggesting greater fibrosis and hypertrophy (Fig. 5a). However, there was no significant difference in the average diameter of the defect site between the two groups (Fig. 5b). ICRS-I and -II scoring from all eight replicates further indicated better repair from the iMPC group than the MSC group (Fig. 5c−e).

The morphology of the samples after 48 weeks of implantation is shown in Supplementary Fig. 5. The most prominent change was the reduction of defect sites from the iMPC group and the severe degradation of

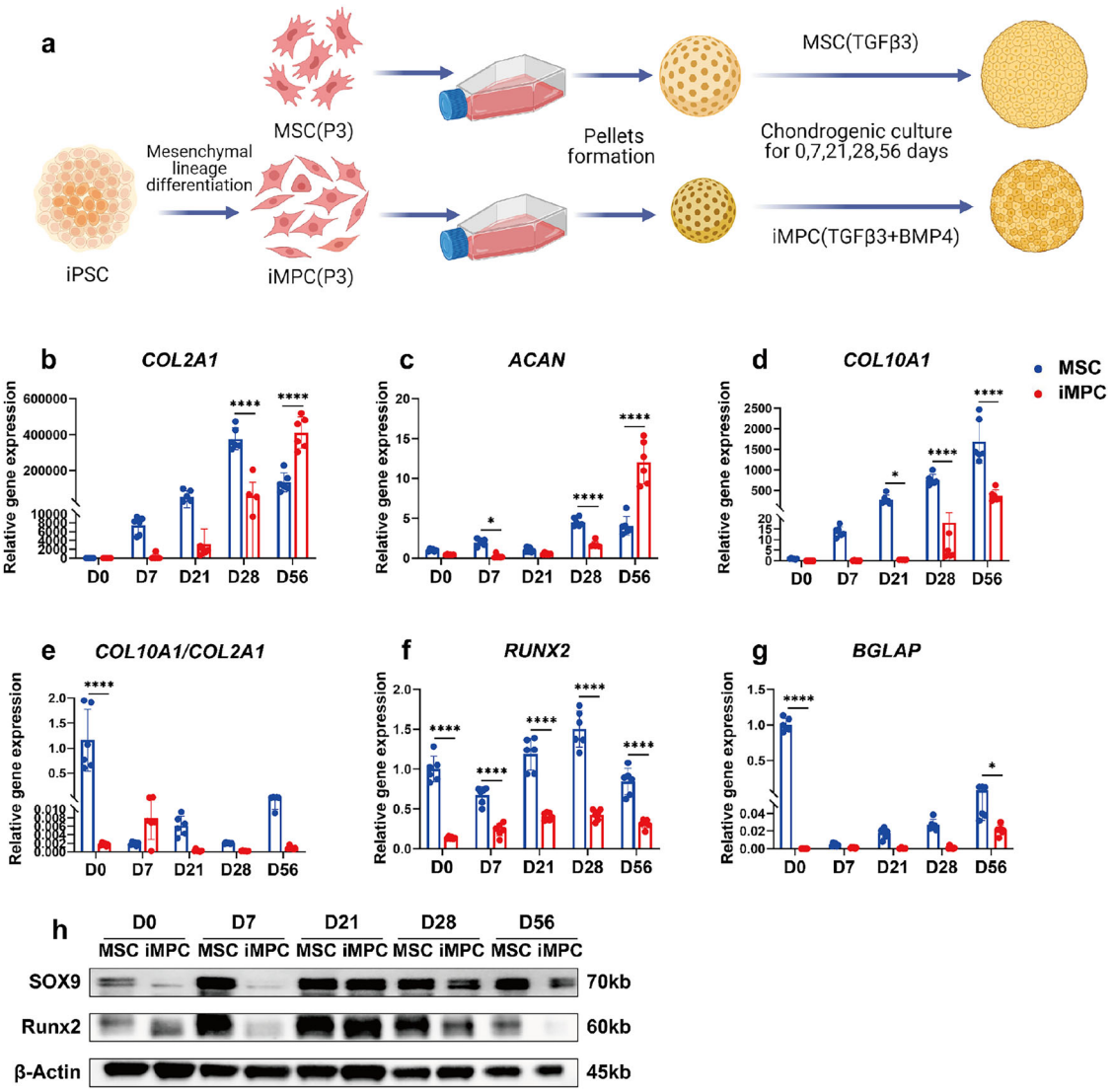

Fig. 1 | Comparison of chondrogenesis of human iPSCs-derived multipotent progenitor cells (iMPCs) and mesenchymal stem cells (MSCs) over time. **a** Schematic representation of procedures to generate cartilage tissues from human iMPCs and MSCs. A basic medium (BM) supplemented with transforming growth factor-beta 3 (TGFβ3) was used to induce MSC chondrogenesis, while BM supplemented with TGFβ3 and bone morphogenetic protein 4 (BMP4) was used to induce iMPC chondrogenesis. **b**–**g** Relative expression levels of chondrogenesis-related markers (COL2A1 and ACAN) and hypertrophy/osteogenesis-related markers (COL10A1, RUNX2, and BGLAP). Gene abbreviations: COL2A1, collagen type II alpha 1 chain; ACAN, aggrecan; COL10A1, collagen type X alpha 1 chain; RUNX2, Runt-related transcription factor 2; BGLAP, bone gamma-carboxyglutamate protein. Data were normalized to D0 in the MSC group. N = 6. **h** Relative protein levels of SOX9 (SRY-box transcription factor 9), Runx2 (Runt-related transcription factor 2), and β-Actin (loading control) in samples from the MSC and iMPC groups were examined by western blot. Two-way ANOVA followed by Sidak's multiple comparisons test was carried out. *$p < 0.05$; ****$p < 0.0001$.

native cartilage in some animals from the MSC group. In Fig. 6a, we showed the samples that displayed the best and worst repairing effects from the two groups. Again, we observed more COL2 and GAGs, and less COL1 and OCN in the iMPC group than in the MSC group. Importantly, animals in the MSC group exhibited more pain (Fig. 6b). In addition, significant native cartilage degradation was observed only in animals from the MSC group. Specifically, the average diameter of defect sites in the MSC group increased from ~1100 μm at 12 weeks to ~1600 μm at 48 weeks (Figs. 5b, 6c). In comparison, the average diameter of defect sites in the iMPC group decreased from ~800 μm at 12 weeks to ~600 μm at 48 weeks. The possible reason might be attributed to the higher levels of MMPs produced by MSC-derived cartilage compared to iMPC (Supplementary Fig. 6). ICRS-I (Fig. 6d) and -II (Fig. 6e-f) scoring from all animals indicated that iMPC-derived cartilage displayed better chondral repair than the MSC group. Importantly, the implanted human cells can still be found after 48 weeks (Supplementary Fig. 7).

Discussion

The potential of iPSC-derived cartilage for repairing chondral defects has been studied in both preclinical models and human clinical trials. However, its long-term efficacy and safety have not yet been fully examined. In this study, we implanted both human MSCs and iPSC-derived cartilage in adult rats, assessing both the implants and surrounding tissues. Our results showed that after 48 weeks (equivalent to 30 years in humans[13]), the cartilage created by MSCs was not able to repair the original chondral defect. Instead, the surrounding host cartilage tissues underwent continuous degradation, resulting in an enlarged defect in some rats. In comparison, although cartilage created by iPSCs also did not fully repair the injuries in all tested animals, surrounding tissues maintained their integrity. Our study indicated the superiority of iPSCs to MSCs in repairing chondral defects.

Regarding the method of differentiating iPSCs into chondrocytes, different protocols have been tested, which were recently summarized by Ali et al.[5]. Our method involved first forming iMPCs through a series of

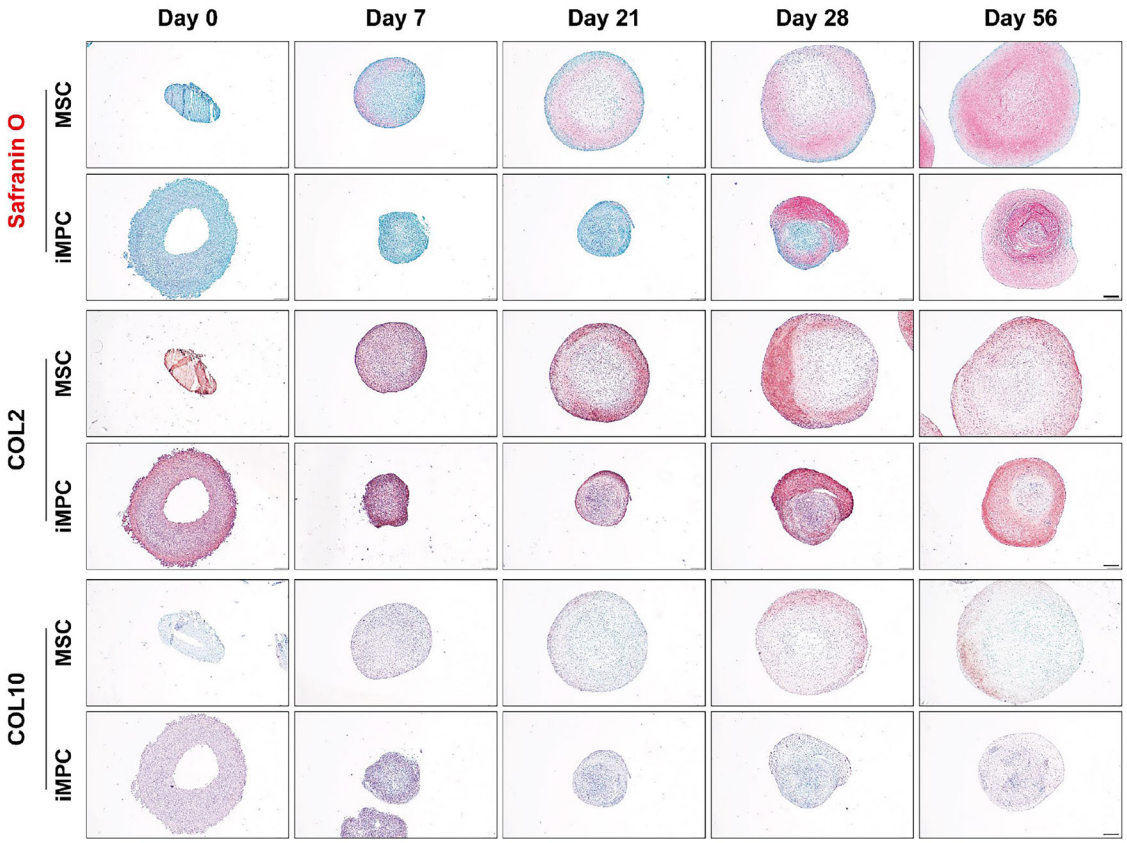

Fig. 2 | Safranin O staining, Collagen Type II (COL2), and Collagen Type X (COL10) immunohistochemical (IHC) to assess the chondrogenesis of MSC and iMPCs at different time points. Scale bar: 200 μm.

monolayer cultures and then inducing them into chondrocytes using pellets. Although some studies indicated the successful chondrogenesis of iMPCs using a medium containing TGFβ[14–16], our results indicated that co-treatment with BMPs was necessary, as other groups reported[17–20]. The reason for this difference is not clear. Of note, in another iPSC differentiation method that formed embryoid bodies (EBs) as an intermediate stage, BMP4 was used to induce EB formation. After that, TGFβ was also sufficient to drive a robust chondrogenesis[6]. Therefore, the activation of BMP pathway is required, either during the generation of progenitor cells[21] or in the differentiation of progenitor cells into chondrocytes[7,22], whether through BMPs or other activators.

The goal of this study was to assess the long-term behavior of iPSC-derived cartilage both in vitro and in vivo. Several studies have reported extended in vitro chondrogenic culture of iPSC-derived constructs, including up to 12 weeks as demonstrated by Raftery et al.[6,16,23–25]. Although a longer time was possible, we selected 56 days in our study for practical reasons. In our previous study that conducted 21-day chondrogenesis, we discovered that the co-treatment of BMP4 + TGFβ3 displayed a comparable efficacy in generating cartilage from iMPCs[8]. Another study indicated that overexpressing BMP-4, along with TGFβ, induced strong chondrogenesis in iPSCs[26]. Our results indicated that BMP-4 was superior to BMP-6 in facilitating iMPC chondrogenesis after 56 days of culture (Supplementary Fig. 2). We also tracked the changes in both MSC and iMPC-derived cartilage at different time points. Importantly, a similar continuous increase of chondrogenic genes in iMPC culture was also observed in a recent study that tested chondrogenesis for 28 days[27–30]. In another study that conducted a 28-day culture, the size of iMPC pellets also grew bigger over time[31]. In addition, more matrix was deposited on day 28 than on day 21, in particular COL2[26]. Collectively, these previous results and our current findings suggest that the time to reach the peak of chondrogenesis from iMPC is longer than that from MSC.

Our results (Fig. 1) again confirmed the findings that iPSC-derived cartilage generally displayed a lower chondrocytic hypertrophy than those from MSCs[8,32]. However, the underlying mechanism is not fully understood. Figure 1h showed that iMPCs expressed significantly lower Runx2, a currently known hypertrophy driver, when compared to MSCs. More importantly, low Runx2 expression was maintained during 56 days of chondrogenesis, which raised the question of why iMPCs display lower Runx2 expression. Gadomski reported that the activation of BMPs at early chondrogenesis may be necessary to achieve a stable hyaline cartilage phenotype[7]. Interestingly, in most differentiation processes from iPSCs to chondrocytes, BMPs are needed either during the process from iPSCs to iMPCs or from iMPCs to chondrocytes. Such a step was not routinely performed in MSC chondrogenesis. However, it is generally accepted that BMPs activate Runx2. Therefore, there must be other mechanisms that suppress the expression of Runx2. In another study by Lamandé et al., chondroprogenitor cells derived from iPSCs underwent hypertrophic differentiation in the absence of TGFβ, whereas the addition of TGFβ promoted the formation of hyaline-like cartilage, underscoring the importance of TGFβ signaling in maintaining the chondrogenic phenotype[33]. Therefore, the presence of TGFβs may be the key, functioning differently in iMPCs and MSCs, but other components may also be involved. For example, Wu discovered that WNTs activation is associated with the formation of off-target hypertrophic cartilage, and the elimination of these cell lineages significantly enhanced the yield and homogeneity of hiPSC-derived chondrocytes[34]. It has been known that WNT inhibitors can reduce the formation of hypertrophy[35,36], and also reduce the expression of Runx2[36]. Lastly, the high density of cell culture may result in rapid acidification and nutrient depletion of the medium, which may also impact the differentiation outcome[37–39].

The chondral repairing capacity of iPSC was also examined in several animal models, including mice, rats, minipigs, and monkeys[7,9,23,40–43]. Given that most recipients of ACI-like cell therapy are young and the regenerated

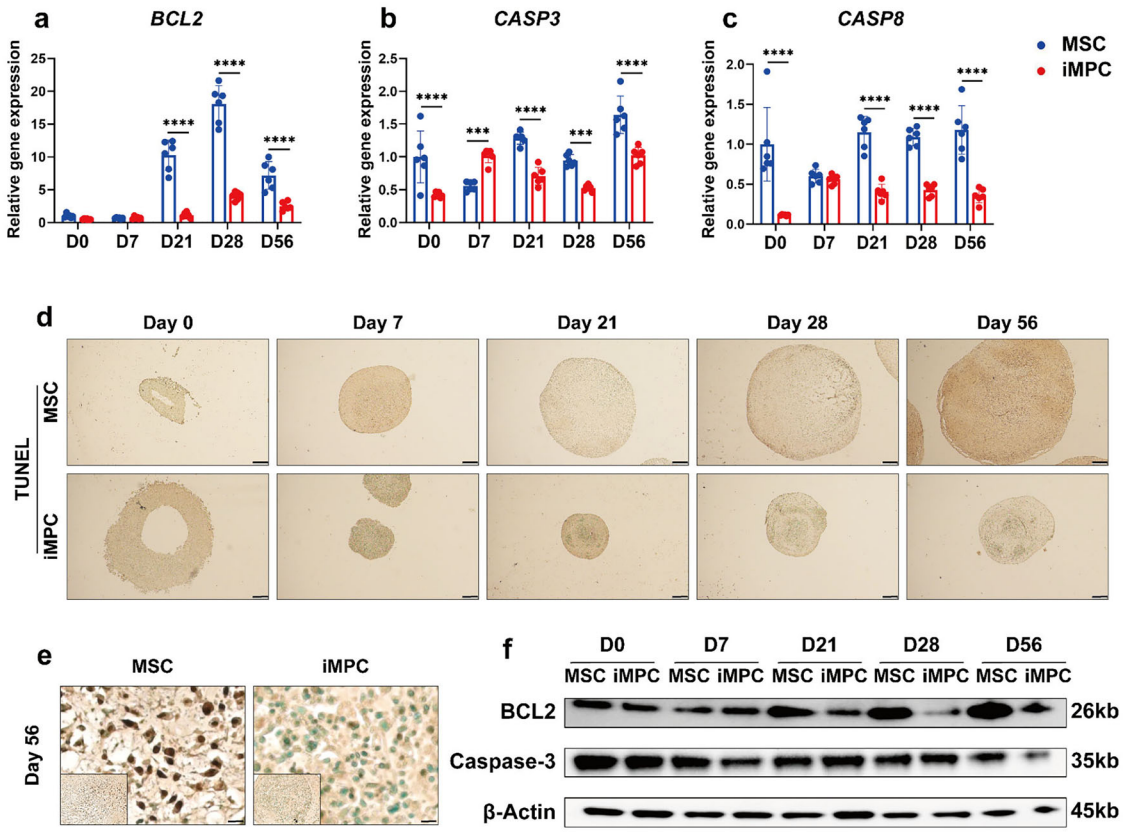

Fig. 3 | Assessment of apoptosis in MSC and iMPC-derived cartilage tissues. **a**–**c** Relative expression levels of apoptosis-related genes (BCL2, CASP3, and CASP8). Gene abbreviations: BCL2, B-cell lymphoma 2; CASP3, Caspase 3; CASP8, Caspase 8. Data were normalized to D0 in the MSC group. N = 6. **d** TUNEL staining at different chondrogenic culture time points. Scale bar: 200 μm. **e** Representative images from TUNEL staining after 56 days of chondrogenic culture. Scale bar: 10 μm. **f** The relative protein levels of BCL2(B-cell lymphoma 2), Caspase3, and β-Actin in MSC and iMPC at different chondrogenic culture time points were examined by western blot (N = 5). Two-way ANOVA followed by Sidak's multiple comparisons test was carried out. ***$p < 0.001$; ****$p < 0.0001$.

cartilage is expected to last for decades, it will be important to estimate the long-term durability of the repair tissue. To the best of our knowledge, the longest in vivo studies were 6 months in mice[9], 24 weeks in rats[42], 4 months in minipigs[43], and 17 weeks in monkeys[41]. The goal of this study was to extend to 48 weeks in rats, which remains one of the longest follow-up durations in rodent cartilage repair studies using iPSC-derived constructs. Furthermore, we used normal rats with intact immune systems to better simulate the conditions of future clinical applications. Articular cartilage is generally considered immune-privileged, and iPSC-derived cartilage tissues generally display low immunity[44]. Previously, implantation of human iPSC-derived cartilage into the subcutaneous tissue of mice, a site that is typically used to test the immunity of cells or implants, caused a mild immune reaction against the xenogeneic cartilage[45]. Moreover, allogeneic iPSC-derived cartilage has been shown to survive, integrate, and remodel as articular cartilage in monkey models[41]. In fact, in a comparative study, iPSC-derived cartilage was no more antigenic than human cartilage[46], and allogenic cartilage and bone have been used to treat osteochondral defects in humans[47–50]. Therefore, these findings, along with our current results, suggest the potential of allograft and xenograft applications of iPSC cartilage for cartilage repair.

Safety is a significant concern when iPSCs are used, given their potential to form tumors. In our study, we did not notice any tumors in the knee joint from the iMPC group. We also collected the major organs, and no tumors were identified (Supplementary Fig. 8). In a previous study using nude rats, the authors concluded that the implantation of 15 g or less of iPSC-derived cartilage in the knee joint does not pose a risk of tumor formation, assuming that the tumorigenic cells from iPSCs are equivalent to HeLa cells and that nude rat knee joints are comparable to human knee joints in terms of tumorigenicity[51]. In fact, 15 g of cartilage would fill a defect area of 68 cm^2, which is larger than most defects seen in knee joint surfaces in clinical settings[51]. Another study reported that an immature teratoma had developed in one mouse after 16 weeks of implantation of iPSC-derived cartilage, possibly due to a relatively short differentiation process[40]. Of note, although most currently tested human embryonic stem cells (ESCs) and most iPSC lines have safely formed cartilage in vivo without causing tumor formation, certain human iPSCs displayed a pro-oncogenic state, as indicated by the presence of secretory tumors during cartilage differentiation in vitro[52]. Therefore, the safety of iPSC-derived cartilage still requires careful evaluation in the future, such as testing more iPSC lines and longer implantation times.

Another unexpected but important finding from this study is the degradation of native cartilage in some rats from the MSC group after 48 weeks, which was not previously reported. Actually, at 12 weeks, we did not notice this phenomenon, indicating that it was a relatively long and continuous process. Several potential reasons could explain this. First, animals housed for 48 weeks had larger knee joints than those only housed for 12 weeks, resulting in enlargement of defects. However, such enlargement is not a necessary consequence since we did not see it in animals from the iMPC group. Second, this was due to the failure of repair from MSC-derived implants, so the continuous use of the injured area may make cartilage degradation faster. Implants from MSCs also produced more proinflammatory cytokines or enzymes that can break down the cartilage matrix (Supplementary Fig. 6). Third, the anti-inflammation or anti-osteoarthritic function of iPSC-derived cartilage reduced the response of tissues to the inflammatory cytokine IL-1β[53], thereby preserving the cartilage tissue after the surgery performed to create the defect. Fourth, RNA sequencing data suggested higher MHC in MSC-derived cartilage (Fig. 4c &d), which may result in T cell

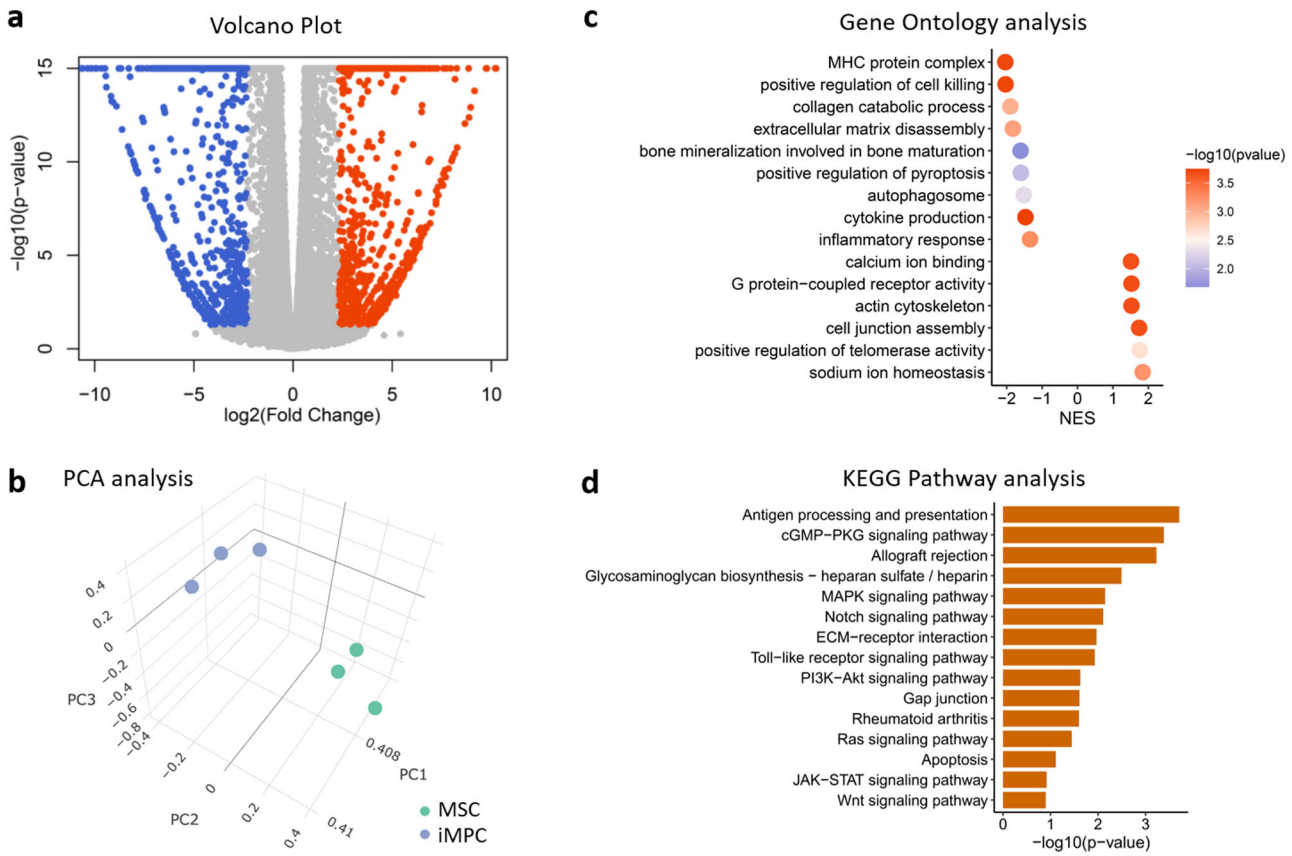

Fig. 4 | Bulk RNA sequencing was performed after MSC and iMPC-derived pellets were differentiated for 56 days. a Genes with differential expression levels greater than five-fold (X-axis) and adjusted p-value < 0.05(Y-axis) were visualized as volcano plot showing the differential expression of 1559 genes. **b** Principal component analysis (PCA) showing segregation of MSC- vs. iMPC-derived chondrocytes. **c** Gene set enrichment analysis using the Gene Ontology (GO) biological process database, with the genes ranked based on their expression fold change of iMPC over MSC. The Y-axis label represents the pathway, and X-axis label represents the normalized enrichment score (NES). Positive NES scores represent activated pathways in MSC group, while negative values represent inhibited ones in MSC group. Color of the bubble shows the -log10 transformed adjusted p-value. MHC= major histocompatibility complex. **d** Kyoto Encyclopedia of Genes and Genomes (KEGG) pathway analysis showing enrichment of molecular pathways resulted from the difference between MSC- and iMPC-derived chondrocytes. cGMP-PKG = Cyclic GMP and cGMP-dependent protein kinase G; MAPK = mitogen-activated protein kinase; ECM = extracellular matrix; PI3K-Akt = phosphatidylinositol 3-kinase - protein kinase B; JAK-STAT = janus kinase/signal transducer and activator of transcription.

infiltration. Last but not least, MSC-derived tissues contained high-level expression of collagen type I, and fibrous cartilage tissues have been shown to degrade faster than hyaline cartilage[54]. The presence of osteocalcin, shown in Figs. 5 & 6, also indicated the inferior property of new cartilage, which can be a sign of osteoarthritis[55].

This study can be further improved in the future. First, we did not compare the reparative capacity of iPSC-derived cartilage after different days of in vitro chondrogenesis. As discussed above, samples from 56 days of differentiation were used since they displayed the most matrix formation. We may test additional points between 21 and 56 days in future animal studies. Second, the mechanisms underlying the difference between MSCs and iMPCs have not been fully studied. In particular, previous studies have shown how the sources of cells affected their efficacy in repairing chondral injury[56,57]. Therefore, the observed difference between MSC and iPSC may be due to the specific donors that were used. In addition, pooled MSCs were used, so it is possible that MSCs from some donors may behave differently from those from others after implantation. The potential impact of cell donors will be explored in the current study. Lastly, we found differences in pain levels between the two groups, which implied pathological changes in other tissues, particularly synovial tissues. In the current study, we did not collect or analyze other joint components (e.g. synovium, meniscus), which limited our ability to fully evaluate the broader impact of the implanted constructs, such as immune response. Future studies will further address these limitations.

Methods

MSC isolation from human bone marrow

With the approval from the Institutional Review Board (IRB) at the University of Pittsburgh and the University of Washington, MSCs were isolated from the femoral heads as previously described[58]. The femoral heads were the surgical waste from total joint replacements. Cells were maintained in a growth medium (GM, DMEM, Gibco, Grand Island, NY) with 1% antibiotic-antimycotic (Gibco) and 10% fetal bovine serum (FBS) (Gemini Bio, West Sacramento, CA). Fibroblast growth factor 2 (FGF2, 1.5 ng/ml) (PeproTech, Hamburg, Germany) was also added into the media during cell expansion. Cell culture media were changed every two days. When reaching 70%–80% confluence, the tissue culture flasks were treated with 0.25% trypsin-ethylenediaminetetraacetic acid (EDTA) (Gibco), and cells were passaged. MSCs were isolated from sixteen de-identified donors. Four were from old females, four were from old males, four were from young females, and four were from young males. Refer to Supplementary Table 1 for more detailed donor information. To complete the study, which required a large number of cells, we used the pooled MSCs from these sixteen donors in pellets culture for cartilage formation.

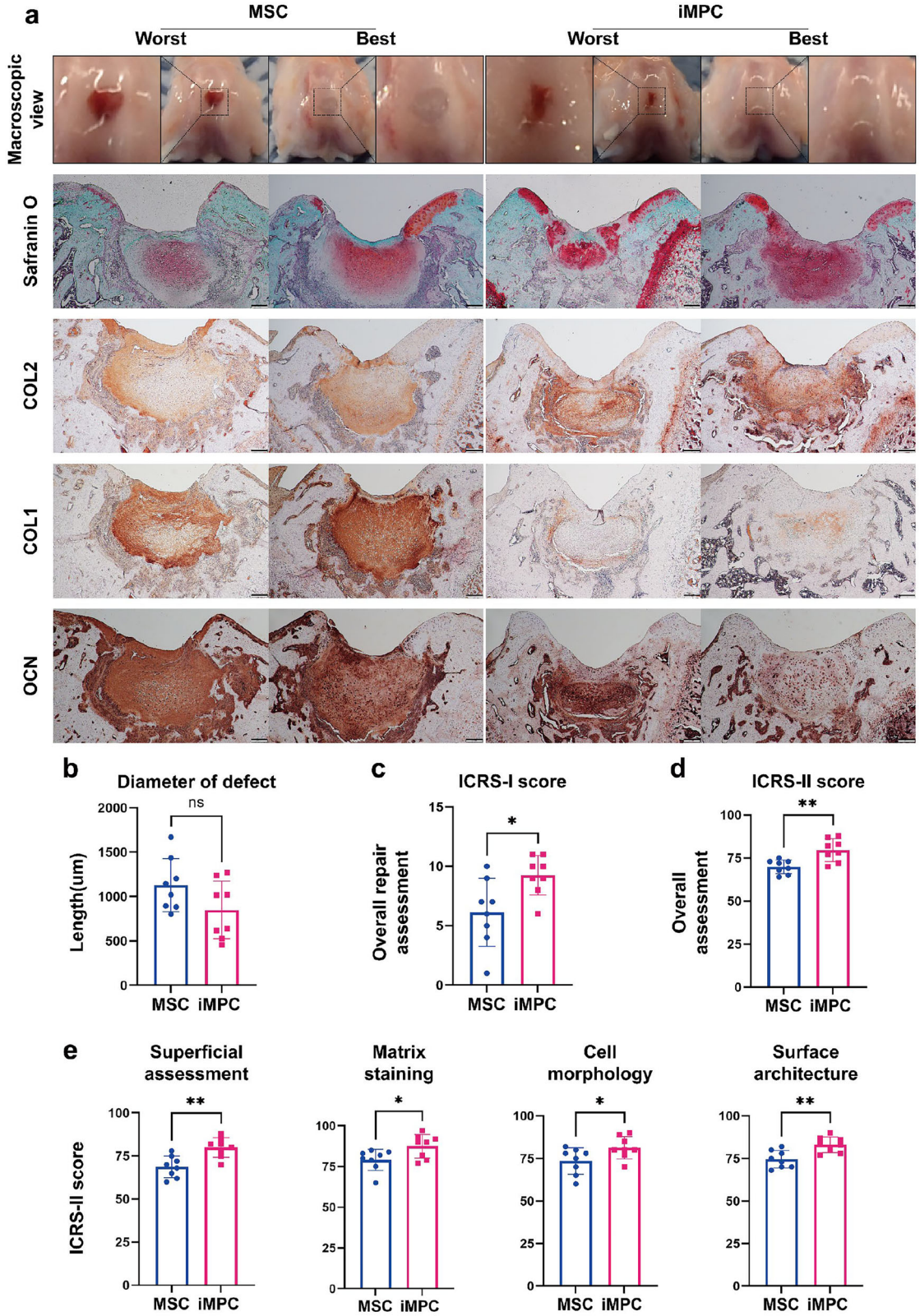

Fig. 5 | Implantation of MSC- or iMPC-derived cartilage in rat joints for 12 weeks. a The samples displaying the worst and best repair from each group are presented. Safranin O staining, and Type II Collagen (COL2), Type I Collagen (COL1), and osteocalcin (OCN) IHC were used to assess the properties of cartilage tissues at the defect site. Scale bar: 200 μm. **b** The diameter of defects was measured using imaging from safranin O staining. Specifically, the longest distance between host tissues around the defect site, with the presence of glycosaminoglycans, was measured and considered as the diameter of the defect site. **c** ICRS-I and (**d**, **e**) ICRS-II scoring for visual assessment and histological assessment of cartilage regeneration, respectively. N = 8 rats. An unpaired t-test was carried out. *$p < 0.05$; **$p < 0.01$.

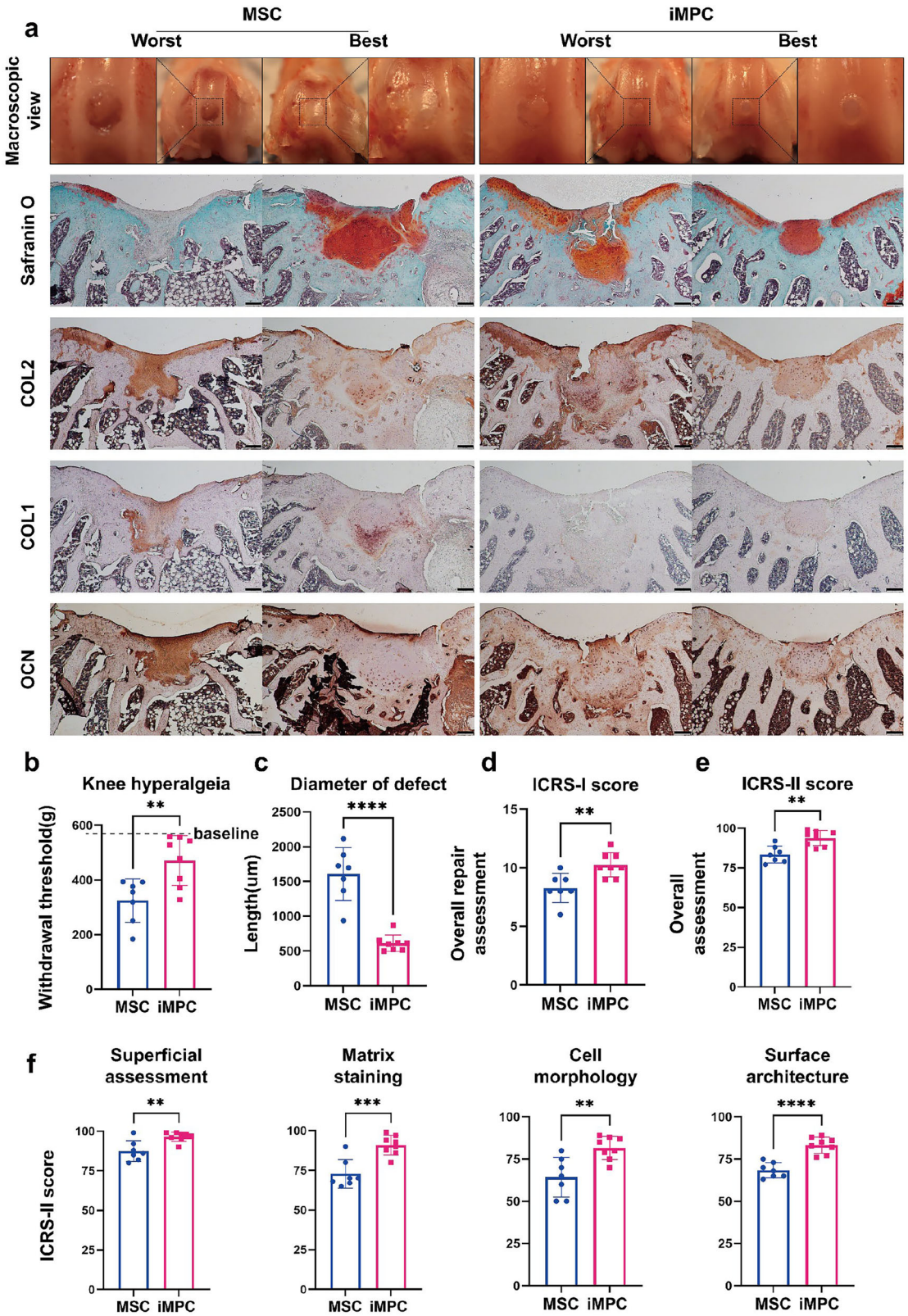

Fig. 6 | Implantation of MSC- or iMPC-derived cartilage in rat joints for 48 weeks. a The samples displaying the worst and best repair from each group were presented. Safranin O staining, and Type II collagen (COL2), Type I collagen (COL1), and Osteocalcin (OCN) IHC were used to assess the properties of cartilage tissues at the defect site. Scale bar: 200 μm. **b** Knee hyperalgesia was assessed with the Pressure Application Measurement (PAM) test. **c** Diameter of defect. **d** ICRS-I scoring for visual assessment of repaired rat joints. **e**, **f** ICRS-II scoring for histological assessment of regenerated cartilage. N = 7 in the MSC group and N = 8 in the iMPC group. An unpaired t-test was carried out. *$p < 0.05$; **$p < 0.01$; ***$p < 0.001$; ****$p < 0.0001$.

Generation of iMPCs from iPSCs

iPSCs were purchased from ALSTEM (Richmond, CA), which were created from umbilical cord-derived MSCs. All media used for expanding and differentiating iPSCs were purchased from STEMCELL Technologies (Vancouver, Canada). As described in the manufacturer's instructions, iPSCs were seeded onto non-tissue culture six-well plates (Corning Life Sciences, Corning, NY) coated with Vitronectin (STEMCELL Technologies). The mTeSR™1 medium was used and was changed daily. Once reaching optimal confluency, iPSCs were detached using ReLeSR (STEMCELL Technologies) or Gentle Cell Dissociation Reagent (STEMCELL Technologies). For passaging purposes, ReLeSR™ was used for detachment, and the iPSCs were re-seeded at the appropriate density with mTeSR™1 medium. To generate iMPCs, iPSCs underwent 3 phases as we did previously[8]. In Phase 1, iPSCs were cultured in mTeSR™1 medium, and iPSCs should be passaged for mesenchymal progenitor induction. On Day 0 of Phase 2, iPSCs were induced into early mesoderm progenitor cells by replacing mTeSR™1 medium with STEMdiff™ Mesenchymal Induction Medium. By Day 4 (Phase 3), STEMdiff™ Mesenchymal Induction Medium was replaced with MesenCult™-ACF Medium to derive early mesenchymal progenitor cells (MPCs). On Day 6, cells were passaged onto cultureware precoated with MesenCult™-ACF Attachment Substrate in MesenCult™-ACF Medium. By Day 21, human iPSC-derived MPCs exhibited the suggested MSC characteristics (Supplementary Fig. 1). When cultures reached ~80% confluence, iMPCs were expanded on tissue culture flasks in the DMEM/F-12 medium (Gibco) supplemented with 10% FBS and 1% antibiotic-antimycotic.

Trilineage differentiation

For osteogenesis, iMPCs were seeded in six-well plates at a density of 20,000 cells/cm² and cultured in osteogenic medium (OM: high-glucose DMEM (Gibco) supplemented with 10% FBS, 1% antibiotic-antimycotic, 0.1 μM dexamethasone, 10 mM β-glycerophosphate, and 50 μg/mL ascorbate 2-phosphate; all from Sigma-Aldrich). After 21 days of induction, iMPCs were fixed in 10% formalin for 15 minutes, rinsed thoroughly with tap water, and stained with 0.5% Alizarin Red solution (pH 4.2, Rowley Biochemical, Danvers, MA) for 5 minutes at room temperature with gentle agitation. Excess dye was removed by aspiration, followed by additional washes with tap water.

For chondrogenesis, iMPCs were seeded as pellets containing 1.5×10^6 cells each and cultured in chondrogenic medium (CM: high-glucose DMEM supplemented with 1% antibiotic-antimycotic, 0.1 μM dexamethasone, 10 μg/mL ITS +, 40 μg/mL L-proline, 50 μg/mL ascorbate 2-phosphate, and 10 ng/mL TGF-β3; all from Sigma-Aldrich or Peprotech) for 21 days. Cells were then fixed in 4% paraformaldehyde for 15 minutes and pretreated with 3% acetic acid for 15 minutes. 0.5% Safranin-O/0.005% Fast green solution was added and incubated at room temperature for 20 minutes to assess glycosaminoglycan deposition.

For adipogenesis, iMPCs were seeded at a density of 20 000 cells/cm2 in six-well plates and cultured for 3 days in Endothelial Cell Growth Basal Medium-2 (EBM-2, Lonza, Walkersville, MD) supplemented with 0.1% FBS, 1% Antibiotics-Antimycotics, 5 mM SB431542 ALK inhibitor (Abcam, Cambridge, MA), 25 mg/mL L-Ascorbic acid 2-phosphate sesquimagnesium salt hydrate (Sigma-Aldrich, St. Louis, MO), 4 mg/mL hydrocortisone (Sigma-Aldrich), 10 ng/mL EGF (Thermo Fisher Scientific, Waltham, MA), 0.5 mM 3-Isobutyl-1-methylxanthine (IBMX, Sigma-Aldrich), 0.25 mM dexamethasone (Sigma-Aldrich), 0.2 nM 3,3′,5-Triiodo-L-thyronine sodium salt (T3, Sigma-Aldrich), 0.1% Insulin-Transferrin-Selenium-Ethanolamine (ITS, Gibco), and 1 mM Rosiglitazone (Sigma-Aldrich), with a media change on day 2. On day 4, iMPCs were cultured in a similar medium (excluding IBMX and dexamethasone) for 21 days with media changes every two days. After 21 days, cells were fixed in 4% paraformaldehyde and stained with Oil Red O to assess lipid accumulation.

Flow cytometry

iMPCs were detached using trypsin, washed, and incubated with FITC-conjugated mouse anti-human antibodies targeting CD73, CD90, CD105, CD31, CD34, and CD45 (BD Biosciences, Franklin Lakes, NJ) to evaluate surface marker expression. For each antibody staining, one million cells were used. Based on the manufacturer's instructions, 5 μL of antibody was added to 100 μL of cell suspension for CD31, CD34, CD45, CD73, CD90, and CD105 detection. Propidium iodide (PI; 1:150 dilution) was used to exclude dead cells. Flow cytometry was performed using a BD FACSAria™ II cell sorter (BD Biosciences, NJ) to assess fluorescence intensity and quantify marker expression. Antibody information can be found in Supplementary Table 3.

Pellet culture and chondrogenesis

Chondrogenic pellet culture was initiated by first resuspending 0.5×10^6 MSCs or 1.5×10^6 iMPCs in 200 μl basic chondrogenic medium (BM, high-glucose DMEM supplemented with 1% antibiotic-antimycotic, 0.1 μM dexamethasone, 40 μg/ml L-proline, 50 μg/ml ascorbic acid, 1×insulin-transferrin-selenium (ITS, Invitrogen, San Diego, CA). Growth factors were added as indicated below. The concentrations of the growth factors were as follows: 10 ng/ml transforming growth factor-beta 3 (TGF-β3, PeproTech), 100 ng/ml bone morphogenetic protein 4 (BMP4, PeproTech) or BMP6 (PeproTech). Cell suspensions were then plated in 96-conical well plates and then centrifuged at $300 \times g$ for 10 min to form pellets. All in vitro chondrogenic differentiation cultures were maintained in a standard humidified incubator that kept CO_2 level at 5%. Oxygen levels were not controlled in all in vitro experiments. The medium was replaced every 2 days, and pellets were harvested after 0, 7, 21, 28, and 56 days for further analysis.

Quantitative Real-time PCR (qRT-PCR)

Total RNA was isolated using Trizol (Life Technologies, Carlsbad, CA), followed by RNA extraction using an RNeasy Plus Universal Kit (Qiagen, Germantown, MD). NanoDrop One microvolume UV-Vis Spectrophotometers (Thermo Fisher Scientific, Waltham, MA) were used to measure total RNA concentration. Reverse transcription was performed with SuperScript™ IV VILO™ Master Mix (Invitrogen). Quantitative real-time polymerase chain reaction was performed using PowerUp™ SYBR™ Green Master Mix (Applied Biosystems, Foster City, CA) according to the manufacturer's instruction. The gene expression levels were calculated using the $2 - \Delta\Delta CT$ method. To determine the expression levels of each gene, CT values were normalized to the housekeeping gene (β-Actin). All primer sequences of target genes (IDT, Newark, NJ) are listed in Supplementary Table 2.

Western blot

Cells were lysed using RIPA buffer (Sigma-Aldrich, Burlington, MA) supplemented with the Halt™ Protease and Phosphatase Inhibitor Cocktail (100×) (Thermo Fisher Scientific) while kept on ice for 15 min. The samples were then centrifuged at 14,000 g for 15 min at 4 °C to collect the supernatant. After that, the soluble protein samples were denatured at 95 °C with 4× Laemmli Sample Buffer (Bio-Rad, Hercules, CA) that contained 10% 2-mercaptoethanol (Bio-Rad). The protein samples were fractionated electrophoretically on NuPAGE™ 4–12% Bis-Tris Gel (Invitrogen) and subsequently transferred to membranes by the semi-dry (Invitrogen) or wet transfer method (Bio-Rad). Following blocking with EveryBlot Blocking Buffer (Bio-Rad), the membranes were incubated with primary antibodies overnight at 4 °C on a shaker. Antibody information is provided in Supplementary Table 3. Following incubation with Goat Anti-Rabbit IgG H&L (HRP) (ab6721, Abcam, Cambridge, MA) at room temperature for one hour and a half, the membranes were incubated with SuperSignal West Dura Extended Duration Substrate (Thermo Fisher Scientific) and imaged using ChemiDoc MP Imaging System (Bio-Rad). Image J was utilized to semi-quantify the blot images.

Histology (Safranin O/Fast green staining and Alizarin red staining)

Pellets were fixed in 4% paraformaldehyde aqueous solution (Electron Microscopy Sciences, Hatfield, PA) and incubated overnight at 4 °C. For staining samples from rats, the whole joint was fixed for 48 hours and then decalcified in Immunocal™ Decalcifier (StatLab, McKinney, TX) for 8 weeks. Samples were dehydrated using gradient ethanol solutions and xylene before being embedded in paraffin (Fisher Scientific, Pittsburgh, PA). Paraffin blocks were sectioned into 6-μm thick sections using a Leica microtome (Model RM 2255). Slides were stained using 0.5% Safranin-O/0.005% Fast green or 2% Alizarin red as previously described[59]. Notably, slides from pellet culture were stained with Safranin-O for 20 minutes, while slides from rats were stained for 2 hours. Imaging was taken using a Nikon Eclipse E800 microscope.

TUNEL staining

The TUNEL staining was performed using a TUNEL Assay Kit (ab206386, Abcam). Pellets were rehydrated in a gradient of ethanol and xylene, followed by permeabilization with Proteinase K. Endogenous peroxidases were quenched using 3% hydrogen peroxide in methanol and then were equilibrated with TdT(Terminal deoxynucleotidyl transferase) Equilibration Buffer. TdT enzyme was applied to label DNA breaks, and the reaction was incubated in a humidified chamber. After terminating the labeling reaction with Stop Buffer, the specimens were blocked with Blocking Buffer and incubated with a conjugate for detection. Finally, the development was achieved using DAB, and the slides were counterstained with Methyl Green. Imaging was conducted using a Nikon Eclipse E800 microscope.

Immunohistochemistry (IHC)

The formalin-fixed paraffin-embedded sections first underwent antigen retrieval based on different antibodies. In this experiment, paraffin-embedded sections were subjected to heat-induced epitope retrieval in sodium citrate buffer (eBioscience, San Diego, CA) at 90 °C for 20 min prior to antibody incubation. Slides were then blocked with 10% horse serum (Abcam) in PBS for one hour, incubated at 4 °C overnight with the primary antibody against collagen type II (COL2, ab34712, Abcam, 1:200 dilution), collagen type I (COL1, ab138492, Abcam, 1:1500 dilution), osteocalcin (OCN, ab93876, Abcam, 1:200 dilution), collagen-type X (COL10, 14-9771-82, Invitrogen, 1:50 dilution). The slides were then incubated with a biotinylated anti-mouse/rabbit immunoglobulin G (IgG) secondary antibody for 1 hour, with signal detection via Vector NovaRED® Substrate Kit, Peroxidase (HRP) (SK-4800, Vector Laboratories, Newark, CA). Mayer's hematoxylin was used for counterstaining (Electron Microscopy Sciences). A Nikon Eclipse E800 microscope was used to image the stained sections. Additional antibody information can be found in Supplementary Table 3.

Bulk RNA-seq data analysis

For bulk RNA-seq experiments, cell pellets made by iMPCs or MSCs were induced in the chondrogenic medium (containing TGFβ3 or TGFβ + BMP4) for 56 days, and then lysed in QIAzol from the RNeasy Plus Mini Kit (Qiagen, Germantown, MD, USA) for RNA extraction. Extracted RNA were quantitated Qubit™ RNA BR Assay Kit (Thermo Fisher Scientific) followed by the RNA quality check using Fragment Analyzer (Agilent Technologies, Santa Clara, CA). For each sample, RNA libraries were prepared from 500 ng RNA using the KAPA mRNA HyperPrep Kit (Roche, Indianapolis, IN) according to manufacturer's protocol, followed by quality check using Fragment Analyzer (Agilent Technologies) and fluorescent quantification on the Infinite F Nano + (Tecan, Männedorf, Switzerland). The libraries were normalized and pooled, and then sequenced using NovaSeq6000 platform (Illumina, San Diego, CA,) to an average of 50 M 100PE reads.

Quality control was first applied to raw RNA sequencing reads by tool FastQC. Low-quality reads and adapter sequences were filtered out by the Trimmomatic tool[60]. Surviving reads were then aligned to the human reference genome hg38 using STAR aligner[61], and gene counts were quantified. Differential expression analysis was performed based on gene counts by R package "DESeq2"[62] and DEGs were selected by adjusted p-value ≤ 0.05 and fold change ≥ 5. These DEGs were then applied to Gene Ontology (GO) and Kyoto Encyclopedia of Genes and Genomes (KEGG) for gene set enrichment analysis (GSEA)[63]. This software employs databases of prebuilt pathways with known genes summarized from previous studies, checks gene ranking based on the expression fold change of iMPC-derived cartilage over MSC, and performs statistical tests to determine the enrichment. Significant pathways were defined by p-value ≤ 0.05. To control the false discovery rate, a stringent FDR cutoff of 5% (adjusted p-value < 0.05) was applied. All RNA-seq analysis tools were run using their default parameter settings unless otherwise specified.

Cartilage repair in a rat osteochondral defect model

The animal study was conducted using a protocol approved by the University of Pittsburgh Institutional Animal Care and Use Committee (IACUC). Rats were purchased from Charles River Laboratories (Wilmington, MA). In this study, 32 male rats, aged 8 weeks, were first anesthetized with 4% isoflurane, and then the right knees were shaved, sterilized, and incised medially. The synovial capsule was cut, and the patella was dislocated to expose the femoral trochlear groove. An osteochondral defect (1.6 mm in diameter and 1.6 mm in depth) was made in the trochlear groove of the femur using an Ideal Micro Drill (CellPoint Scientific, Gaithersburg, MD), followed by irrigation and debris removal. MSC or iMPC-derived cartilage tissues were inserted into defect sites by press-fit. It should be noted that pellets from the iMPC culture were significantly smaller than those from the MSC culture on day 28. If we used constructs at this point, several iMPC pellets would be required per defect site, while only one MSC pellet was needed. This would make these two groups incomparable. Therefore, we selected the constructs for implantation after 56 days of chondrogenesis. After implantation, the patella was repositioned to its original anatomical location, and the subcutaneous layer and skin were closed with 4-0 suture.

After 12 weeks and 48 weeks, the rats were euthanized with carbon dioxide (CO2), followed by decapitation to ensure an irreversible death. Eight rats were included in each group, but one rat died from the MSC group at week 37. Knees were fixed in a 4% paraformaldehyde aqueous solution for 48 h and then decalcified by Immunocal™ Decalcifier for 8 weeks. After that, samples underwent sequential dehydration in different concentrations of ethanol (from 20%, 50%, 70%, 95% to 100%) for 2 h each, cleared in xylene for 2 h and embedded in paraffin. Paraffin blocks were sectioned into 6 μm-thick sections. IHC and histology staining were performed as described above. The visual and histological assessments of specimen images were performed to evaluate the repair of cartilage defects. Briefly, macrographs and micrographs of reconstructed cartilage were blindly scored by four independent reviewers following the ICRS-I (https://cartilage.org/) and ICRS-II[64] scoring systems, respectively. For visual assessment, macrographs of femoral condyles were scored on the categories of integration to the border zone, macroscopic appearance, and degree of defect repair. For histological assessment, micrographs of regenerated cartilage defects were scored on four different evaluation categories. Each score presented in the results was calculated as the mean of the four independent reviewers' scores.

Knee hyperalgesia

Knee hyperalgesia was measured after 48 weeks of implantation using a Pressure Application Measurement (PAM) device (Ugo Basile, Varese, Italy). Rats were restrained by hand, and the hind paw was lightly pinned to make the knee flexion similar to that of each rat. The PAM transducer was pressed against the medial side of the knee. PAM software guided the user to apply a constantly increasing force (30 g/s) up to a maximum of 500 g. If the rat tried to withdraw its knee, the force at which this occurred was recorded. Two measurements were taken and recorded per knee by an experimenter blinded to the rat strain, and the withdrawal force data were averaged. If rats did not withdraw their knee, a force of 500 g was assigned.

Statistical analyses

Statistical analyses were carried out using GraphPad Prism 9 (GraphPad, San Diego, CA). All data are presented as means and 95% confidence intervals for analyzing the correlation of gene expression. Mean differences between the two groups were assessed using the Student's t-test. Analysis of variance (ANOVA) was used to analyze results among multiple groups. p values less than 0.05 were considered statistically significant and depicted in figures as $*p < 0.05$, $**p < 0.01$, $***p < 0.001$, and $****p < 0.0001$.

Data availability

The transcriptome sequencing data were deposited to the Gene Expression Omnibus with accession ID GSE288164. Both raw sequencing and gene expression profiles can be downloaded through https://www.ncbi.nlm.nih.gov/geo/query/acc.cgi?&acc=GSE288164.

Code availability

In this work, only public software and custom code were used to generate or process datasets. The software version and websites were described in the "Methods" section.

Received: 29 January 2025; Accepted: 2 December 2025;
Published online: 25 December 2025

References

1. Negoro, T., Takagaki, Y., Okura, H. & Matsuyama, A. Trends in clinical trials for articular cartilage repair by cell therapy. *npj Regen. Med.* **3**, 17 (2018).
2. Fellows, C. R., Matta, C., Zakany, R., Khan, I. M. & Mobasheri, A. Adipose, bone marrow and synovial joint-derived mesenchymal stem cells for cartilage repair. *Front. Genet.* **7**, 213 (2016).
3. Mamachan, M. et al. Mesenchymal stem cells for cartilage regeneration: Insights into molecular mechanism and therapeutic strategies. *Tissue Cell* **88**, 102380 (2024).
4. Owaidah, A. Y. Induced pluripotent stem cells in cartilage tissue engineering: a literature review. *Biosci. Rep.* **44**, https://doi.org/10.1042/BSR20232102 (2024).
5. Ali, E. A. M. et al. iPSCs chondrogenic differentiation for personalized regenerative medicine: a literature review. *Stem Cell Res. Ther.* **15**, 185 (2024).
6. Raftery, R. M., Pregizer, S. K., Kocher, S. & Craft, A. M. Regenerative capacity of human pluripotent stem cell-derived articular chondrocytes in vitro. *J. Orthop. Res.* **42**, 1841–1851 (2024).
7. Gadomski, S. J. et al. Time- and cell-specific activation of BMP signaling restrains chondrocyte hypertrophy. *iScience* **27**, 110537 (2024).
8. Xiang, S. et al. Differences in the intrinsic chondrogenic potential of human mesenchymal stromal cells and iPSC-derived multipotent cells. *Clin. Transl. Med.* **12**, e1112 (2022).
9. Kawata, M. et al. Simple and robust differentiation of human pluripotent stem cells toward chondrocytes by two small-molecule compounds. *Stem Cell Rep.* **13**, 530–544 (2019).
10. Park, Y. B., Ha, C. W., Lee, C. H., Yoon, Y. C. & Park, Y. G. Cartilage regeneration in osteoarthritic patients by a composite of allogeneic umbilical cord blood-derived mesenchymal stem cells and hyaluronate hydrogel: results from a clinical trial for safety and proof-of-concept with 7 years of extended follow-up. *Stem Cells Transl. Med.* **6**, 613–621 (2017).
11. Quinn, R. Comparing rat's to human's age: How old is my rat in people years? *Nutrition* **21**, 775–777 (2005).
12. Hallett, S. A., Ono, W. & Ono, N. The hypertrophic chondrocyte: to be or not to be. *Histol. Histopathol.* **36**, 1021–1036 (2021).
13. Sengupta, P. The laboratory rat: relating its age with human's. *Int. J. Prev. Med.* **4**, 624–630 (2013).
14. Khan, N. M., Diaz-Hernandez, M. E. & Drissi, H. Differentiation of human induced pluripotent stem cells (iPSCs)-derived mesenchymal progenitors into chondrocytes. *Bio. Protoc.* **13**, e4874 (2023).
15. Kreuser, U., Buchert, J., Haase, A., Richter, W. & Diederichs, S. Initial WNT/beta-catenin activation enhanced mesoderm commitment, extracellular matrix expression, cell aggregation and cartilage tissue yield from induced pluripotent stem cells. *Front. Cell Dev. Biol.* **8**, 581331 (2020).
16. Diederichs, S., Klampfleuthner, F. A. M., Moradi, B. & Richter, W. Chondral differentiation of induced pluripotent stem cells without progression into the endochondral pathway. *Front. Cell Dev. Biol.* **7**, 270 (2019).
17. Xu, M., Shaw, G., Murphy, M. & Barry, F. Induced pluripotent stem cell-derived mesenchymal stromal cells are functionally and genetically different from bone marrow-derived mesenchymal stromal cells. *Stem Cells* **37**, 754–765 (2019).
18. Lepage, S. I. et al. Generation, characterization, and multilineage potency of mesenchymal-like progenitors derived from equine induced pluripotent stem cells. *Stem Cells Dev.* **25**, 80–89 (2016).
19. Guzzo, R. M., Gibson, J., Xu, R. H., Lee, F. Y. & Drissi, H. Efficient differentiation of human iPSC-derived mesenchymal stem cells to chondroprogenitor cells. *J. Cell Biochem.* **114**, 480–490 (2013).
20. Lee, M. S. et al. Comparative evaluation of isogenic mesodermal and ectomesodermal chondrocytes from human iPSCs for cartilage regeneration. *Sci. Adv.* **7**, https://doi.org/10.1126/sciadv.abf0907 (2021).
21. Dicks, A. R., Steward, N., Guilak, F. & Wu, C. L. Chondrogenic differentiation of human-induced pluripotent stem cells. *Methods Mol. Biol.* **2598**, 87–114 (2023).
22. Li, C. et al. Directed differentiation of human pluripotent stem cells into articular cartilage reveals effects caused by absence of WISP3, the gene responsible for progressive pseudorheumatoid arthropathy of childhood. *Ann. Rheum. Dis.* **82**, 1547–1557 (2023).
23. Yamashita, A. et al. Generation of scaffoldless hyaline cartilaginous tissue from human iPSCs. *Stem Cell Rep.* **4**, 404–418 (2015).
24. Whitney, G. A. et al. Thyroxine increases collagen type II expression and accumulation in scaffold-free tissue-engineered articular cartilage. *Tissue Eng. Part A* **24**, 369–381 (2018).
25. Lach, M. S. et al. Chondrogenic differentiation of pluripotent stem cells under controllable serum-free conditions. *Int. J. Mol. Sci.* **20**, https://doi.org/10.3390/ijms20112711 (2019).
26. Zhang, M. et al. Rapid and efficient generation of cartilage pellets from mouse induced pluripotent stem cells by transcriptional activation of BMP-4 with shaking culture. *J. Tissue Eng.* **13**, 20417314221114616 (2022).
27. Tong, X. et al. Isolation and tracing of matrix-producing notochordal and chondrocyte cells using ACAN-2A-mScarlet reporter human iPSC lines. *Sci. Adv.* **10**, eadp3170 (2024).
28. Hajmousa, G. et al. The role of DNA methylation in chondrogenesis of human iPSCs as a stable marker of cartilage quality. *Clin. Epigenet.* **16**, 141 (2024).
29. Khan, N. M. et al. Differential chondrogenic differentiation between iPSC derived from healthy and OA cartilage is associated with changes in epigenetic regulation and metabolic transcriptomic signatures. *Elife* **12**, https://doi.org/10.7554/eLife.83138 (2023).
30. Xu, L. et al. Alterations of glycosphingolipid glycans and chondrogenic markers during differentiation of human induced pluripotent stem cells into chondrocytes. *Biomolecules* **10**, https://doi.org/10.3390/biom10121622 (2020).
31. Wei, X. et al. A human organoid drug screen identifies alpha2-adrenergic receptor signaling as a therapeutic target for cartilage

regeneration. *Cell Stem Cell*. https://doi.org/10.1016/j.stem.2024.09.001 (2024).
32. Rodriguez Ruiz, A. et al. Cartilage from human-induced pluripotent stem cells: comparison with neo-cartilage from chondrocytes and bone marrow mesenchymal stromal cells. *Cell Tissue Res.* **386**, 309–320 (2021).
33. Lamande, S. R. et al. Modeling human skeletal development using human pluripotent stem cells. *Proc. Natl. Acad. Sci. USA* **120**, e2211510120 (2023).
34. Wu, C. L. et al. Single cell transcriptomic analysis of human pluripotent stem cell chondrogenesis. *Nat. Commun.* **12**, 362 (2021).
35. Hsieh, C. C. et al. Wnt antagonism without TGFbeta induces rapid MSC chondrogenesis via increasing AJ interactions and restricting lineage commitment. *iScience* **26**, 105713 (2023).
36. Deng, Y. et al. Engineering hyaline cartilage from mesenchymal stem cells with low hypertrophy potential via modulation of culture conditions and Wnt/beta-catenin pathway. *Biomaterials* **192**, 569–578 (2019).
37. Buxton, A. N., Bahney, C. S., Yoo, J. U. & Johnstone, B. Temporal exposure to chondrogenic factors modulates human mesenchymal stem cell chondrogenesis in hydrogels. *Tissue Eng. Part A* **17**, 371–380 (2011).
38. Ullah, M., Hamouda, H., Stich, S., Sittinger, M. & Ringe, J. A reliable protocol for the isolation of viable, chondrogenically differentiated human mesenchymal stem cells from high-density pellet cultures. *BioRes. Open Access* **1**, 297–305 (2012).
39. Pattappa, G., Heywood, H. K., de Bruijn, J. D. & Lee, D. A. The metabolism of human mesenchymal stem cells during proliferation and differentiation. *J. Cell Physiol.* **226**, 2562–2570 (2011).
40. Saito, T. et al. Hyaline cartilage formation and tumorigenesis of implanted tissues derived from human induced pluripotent stem cells. *Biomed. Res.* **36**, 179–186 (2015).
41. Abe, K. et al. Engraftment of allogeneic iPS cell-derived cartilage organoid in a primate model of articular cartilage defect. *Nat. Commun.* **14**, 804 (2023).
42. Nakagawa, S. et al. Repair of osteochondral defects: efficacy of a tissue-engineered hybrid implant containing both human MSC and human iPSC-cartilaginous particles. *npj Regen. Med.* **8**, 59 (2023).
43. Lee, M.-S. et al. Autologous iPSC- and MSC-derived chondrocyte implants for cartilage repair in a miniature pig model. *bioRxiv*, 2023.2007.2025.550409, https://doi.org/10.1101/2023.07.25.550409 (2023).
44. Abe, K. & Tsumaki, N. Regeneration of joint surface defects by transplantation of allogeneic cartilage: application of iPS cell-derived cartilage and immunogenicity. *Inflamm. Regen.* **43**, 56 (2023).
45. Uto, S. et al. Subcutaneously transplanted fresh cartilage in allogeneic and xenogeneic immunocompetent mouse. *Tissue Eng. Part A* **29**, 541–556 (2023).
46. Kimura, T., Yamashita, A., Ozono, K. & Tsumaki, N. Limited immunogenicity of human induced pluripotent stem cell-derived cartilages. *Tissue Eng. Part A* **22**, 1367–1375 (2016).
47. Gracitelli, G. C. et al. Fresh osteochondral allograft transplantation for isolated patellar cartilage injury. *Am. J. Sports Med.* **43**, 879–884 (2015).
48. Murphy, R. T., Pennock, A. T. & Bugbee, W. D. Osteochondral allograft transplantation of the knee in the pediatric and adolescent population. *Am. J. Sports Med.* **42**, 635–640 (2014).
49. Meric, G., Gracitelli, G. C., Görtz, S., De Young, A. J. & Bugbee, W. D. Fresh osteochondral allograft transplantation for bipolar reciprocal osteochondral lesions of the knee. *Am. J. Sports Med.* **43**, 709–714 (2015).
50. Bouz, T. S., Wang, T., Penn, J. K., McCauley, J. C. & Bugbee, W. D. Midterm Survivorship and Clinical Outcomes in Fresh Osteochondral Allograft Transplantation for the Treatment of Large Bipolar Lesions of the Knee. *Am. J. Sports Med.* **53**, 855–862 (2025).
51. Takei, Y. et al. Quality assessment tests for tumorigenicity of human iPS cell-derived cartilage. *Sci. Rep.* **10**, 12794 (2020).
52. Yamashita, A. et al. Cartilage tissue engineering identifies abnormal human induced pluripotent stem cells. *Sci. Rep.* **3**, 1978 (2013).
53. Lee, J., Smeriglio, P., Chu, C. R. & Bhutani, N. Human iPSC-derived chondrocytes mimic juvenile chondrocyte function for the dual advantage of increased proliferation and resistance to IL-1β. *Stem Cell Res Ther.* **8**, 244 (2017).
54. Armiento, A. R., Alini, M. & Stoddart, M. J. Articular fibrocartilage—Why does hyaline cartilage fail to repair? *Adv. Drug Deliv. Rev.* **146**, 289–305 (2019).
55. Pullig, O., Weseloh, G., Ronneberger, D., Kakonen, S. & Swoboda, B. Chondrocyte differentiation in human osteoarthritis: expression of osteocalcin in normal and osteoarthritic cartilage and bone. *Calcif. Tissue Int.* **67**, 230–240 (2000).
56. Tee, C. A. et al. Metabolic modulation to improve MSC expansion and therapeutic potential for articular cartilage repair. *Stem Cell Res. Ther.* **15**, 308 (2024).
57. Česnik, A. B. & Švajger, U. The issue of heterogeneity of MSC-based advanced therapy medicinal products-a review. *Front. Cell Dev. Biol.* **12**, 1400347 (2024).
58. Xiang, S. et al. Caveolin-1 mediates soft scaffold-enhanced adipogenesis of human mesenchymal stem cells. *Stem Cell Res. Ther.* **12**, 347 (2021).
59. Liu, Y., Kuang, B., Rothrauff, B. B., Tuan, R. S. & Lin, H. Robust bone regeneration through endochondral ossification of human mesenchymal stem cells within their own extracellular matrix. *Biomaterials* **218**, 119336 (2019).
60. Bolger, A. M., Lohse, M. & Usadel, B. Trimmomatic: a flexible trimmer for Illumina sequence data. *Bioinformatics* **30**, 2114–2120 (2014).
61. Dobin, A. et al. STAR: ultrafast universal RNA-seq aligner. *Bioinformatics* **29**, 15–21 (2013).
62. Love, M. I., Huber, W. & Anders, S. Moderated estimation of fold change and dispersion for RNA-seq data with DESeq2. *Genome Biol.* **15**, 550 (2014).
63. Subramanian, A. et al. Gene set enrichment analysis: a knowledge-based approach for interpreting genome-wide expression profiles. *Proc. Natl. Acad. Sci. USA* **102**, 15545–15550 (2005).
64. Mainil-Varlet, P. et al. A new histology scoring system for the assessment of the quality of human cartilage repair: ICRS II. *Am. J. Sports Med.* **38**, 880–890 (2010).

Acknowledgements

This work was supported by the Department of Orthopaedic Surgery and the Orland Bethel Family Musculoskeletal Research Center (BMRC) at the University of Pittsburgh School of Medicine. It was also partially supported by Albert B. Ferguson, Jr., M.D. Orthopaedic Fund (to HL and MVH). The funding agencies specifically disclaim responsibility for any analyses, interpretations, or conclusions. YL is a medical student at the Central South University School of Medicine and a visiting research scholar at the University of Pittsburgh School of Medicine, supported by the Central South University Xiangya School of Medicine. RNA sequencing was conducted by the High Throughput Genomics Core (HTGC) at the University of Pittsburgh.

Author contributions

Y.L. designed and performed experiments, analyzed data, and wrote the paper. E.R.K. performed experiments and analyzed data. S.E.H. performed experiments. J.S. performed experiments. S.K. performed experiments. J.L. analyzed data. S.L. analyzed data and edited the paper. M.V.H. conceptualized this study, designed experiments, and analyzed data. H.L.

conceptualized the study, designed experiments, analyzed data, and wrote the paper. All authors have approved the final version of the paper.

Competing interests
The authors declare no competing interests.

Additional information
Supplementary information The online version contains supplementary material available at https://doi.org/10.1038/s41536-025-00447-6.

Correspondence and requests for materials should be addressed to MaCalus V. Hogan or Hang Lin.